BIOCHEMISTRY
including biophysical chemistry & molecular biology

Article

pubs.acs.org/biochemistry

Removal of the C-Terminal Regulatory Domain of α-Isopropylmalate Synthase Disrupts Functional Substrate Binding

Frances H. A. Huisman,[†] Nayden Koon,[‡] Esther M. M. Bulloch,[‡] Heather M. Baker,[‡] Edward N. Baker,[‡] Christopher J. Squire,*[,‡] and Emily J. Parker*[,†]

[†]Biomolecular Interaction Centre and Department of Chemistry, University of Canterbury, Christchurch, New Zealand

[‡]Maurice Wilkins Centre for Molecular Biodiscovery, School of Biological Sciences, University of Auckland, Auckland, New Zealand

Supporting Information

ABSTRACT: α-Isopropylmalate synthase (α-IPMS) catalyzes the metal-dependent aldol reaction between α-ketoisovalerate (α-KIV) and acetyl-coenzyme A (AcCoA) to give α-isopropylmalate (α-IPM). This reaction is the first committed step in the biosynthesis of leucine in bacteria. α-IPMS is homodimeric, with monomers consisting of $(\beta/\alpha)_8$ barrel catalytic domains fused to a C-terminal regulatory domain, responsible for binding leucine and providing feedback regulation for leucine biosynthesis. In these studies, we demonstrate that removal of the regulatory domain from the α-IPMS enzymes of both *Neisseria meningitidis* (*Nme*IPMS) and *Mycobacterium tuberculosis* (*Mtu*IPMS) results in enzymes that are unable to catalyze the formation of α-IPM, although truncated *Nme*IPMS was still able to slowly hydrolyze AcCoA. The lack of catalytic activity of these truncation variants was confirmed by complementation studies with *Escherichia coli* cells lacking the α-IPMS gene, where transformation with the plasmids encoding the truncated α-IPMS enzymes was not able to rescue α-IPMS activity. X-ray crystal structures of both truncation variants reveal that both proteins are dimeric and that the catalytic sites of the proteins are intact, although the divalent metal ion that is thought to be responsible for activating substrate α-KIV is displaced slightly relative to its position in the substrate-bound, wild-type structure. Isothermal titration calorimetry and WaterLOGSY nuclear magnetic resonance experiments demonstrate that although these truncation variants are not able to catalyze the reaction between α-KIV and AcCoA, they are still able to bind the substrate α-KIV. It is proposed that the regulatory domain is crucial for ensuring protein dynamics necessary for competent catalysis.

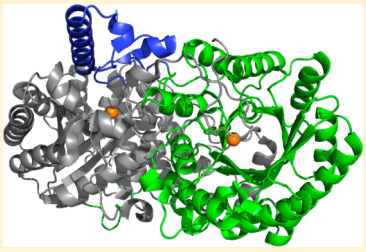

One of the most fascinating aspects of enzymes is how exquisitely they are regulated within metabolic pathways. A key method of such regulation is the binding of pathway end products to specific allosteric binding sites located far from where catalysis takes place. Structural studies have shown that for some enzymes the distances between the binding sites for the allosteric inhibitor and substrates can be quite large, and that the allosteric ligand binding sites can be formed by distinct regulatory domains that are appended to the core catalytic structure.[1,2] In some cases, the regulatory domain acts quite independently of the active site and may be removed to give an unregulated enzyme.[3,4] What are harder to investigate, however, are enzymes for which the removal of a structurally distinct regulatory domain dramatically alters catalytic activity. For these enzymes, contributions to catalysis of this regulatory architecture need to be better understood.

One such allosterically regulated enzyme is α-isopropylmalate synthase (α-IPMS, EC 2.3.3.13), a member of the Claisen condensing family. α-IPMS catalyzes the condensation of α-ketoisovalerate (α-KIV) and acetyl-coenzyme A (AcCoA) to form (*S*)-α-isopropylmalate [α-IPM (Figure 1)]. This is the first committed step in the biosynthesis of leucine, and the enzyme is feedback-inhibited by this amino acid, which binds to an allosteric regulatory domain.[5,6] Most characterized α-IPMS enzymes are homodimeric,[7−9] although some may adopt a tetrameric form.[5,10] All α-IPMS enzymes are reported

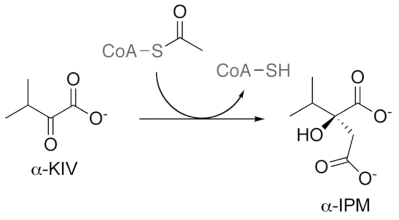

Figure 1. Reaction catalyzed by α-IPMS.

to be dependent on a divalent metal ion for full activity, and some also require a monovalent cation.[11]

Crystal structures of α-IPMS from *Mycobacterium tuberculosis* (*Mtu*IPMS) have defined the binding sites of α-KIV and leucine, but the leucine-bound and leucine-free structures overlay so closely that it is not possible to deduce how effector binding may inhibit catalysis. This protein is a homodimer of 70 kDa monomers, each with an $(\beta/\alpha)_8$ barrel catalytic domain and a βαβ sandwich regulatory domain.[8] Two subdomains and a flexible linker region separate the catalytic and regulatory domains (Figure 2). α-KIV and a Zn^{2+} ion bind at the C-terminal end of the $(\beta/\alpha)_8$ barrel, and leucine binds at the

Received: November 16, 2011
Revised: February 3, 2012
Published: February 21, 2012

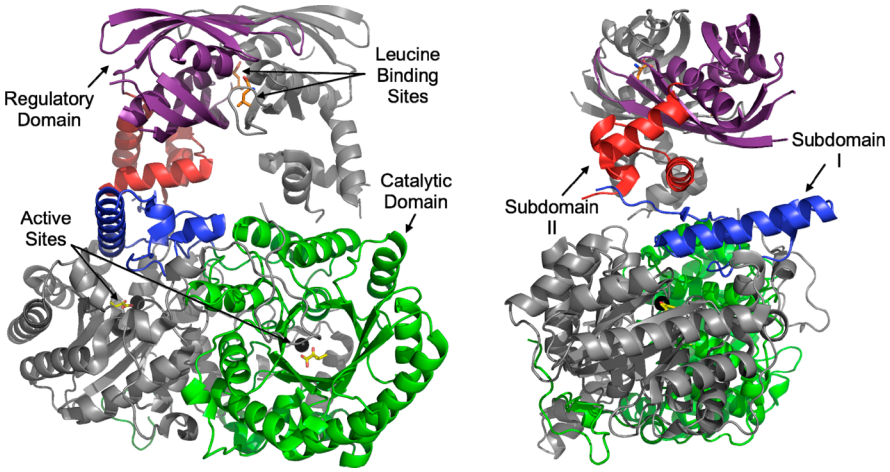

Figure 2. Crystal structure 1SR9,[8] α-IPMS from *M. tuberculosis*. One monomer is colored gray and the other color-coded by domain as follows: green for the catalytic domain, blue for subdomain I, red for subdomain II, and purple for the regulatory domain. α-KIV (yellow) and Zn^{2+} (black) are shown in the active sites. Leucine (orange) has been overlaid from structure 3FIG (leucine-bound *Mtu*IPMS).

interface of the two regulatory domains. Modeling studies predict that AcCoA binds in a pocket on the *re* face of α-KIV, but no structures with this substrate bound have been determined.

The *Mtu*IPMS dimer is domain-swapped such that the subdomains and the regulatory domain of one monomer are adjacent to the $(\beta/\alpha)_8$ barrel of the other monomer. An α-helix of one monomer sits over the active site of the other and contributes two active site residues, His379 and Tyr410.[8] Site-specific replacement of this latter residue was found to uncouple the effect of leucine binding on catalysis, so these residues may play a key role in leucine-mediated regulation.[12] Several mutations in the regulatory domain of *Saccharomyces cerevisiae* α-IPMS have also resulted in insensitivity to leucine.[13]

Because of the lack of a structural explanation for the inhibition of α-IPMS by leucine, it seems probable that allosteric inhibition is primarily driven by changes in protein dynamics, as investigated by Frantom et al.[14] Solution-phase hydrogen−deuterium exchange experiments with the *M. tuberculosis* enzyme have shown that regions in the regulatory domain, subdomain II, and the active site undergo changes in molecular dynamics upon leucine binding. It is proposed that subdomain I, which shows no change in conformational equilibrium upon leucine binding, may act as a node in the allosteric network.

We have shown recently that the regulatory domain of *Neisseria meningitidis* α-IPMS (*Nme*IPMS) is critical for catalytic activity and may be important for positioning of active site residues.[9]

This study compares crystal structures of truncated and full-length α-IPMS enzymes from both *N. meninigitidis* and *M. tuberculosis* to assess the role of the regulatory domain in providing catalytic function. Loss of the C-terminal regulatory domain for both enzymes results in the complete loss of normal catalytic function, despite limited structural changes to the active sites of both truncated proteins.

MATERIALS AND METHODS

Cloning. Plasmids containing *Nme*IPMS (pFH01) and *Mtu*IPMS (pProExHTa-LeuA) were already available from previous work.[9,15] Quikchange site-directed mutagenesis (Stratagene) was used to insert a stop codon at residue Glu365 of *Nme*IPMS in the pFH01 plasmid to give *Nme*E365Term. Glu365 was chosen as it is upstream of the regulatory domain, not highly conserved, and located in a disordered loop of the *Mtu*IPMS structure. Residues 1−425 were amplified from plasmid pProExHTa-LeuA using Platinum *Pfx* DNA polymerase (Invitrogen) to give *Mtu*LeuA425. The resulting polymerase chain reaction product and vector pProExHta were digested with restriction enzymes *Nco*I and *Hin*dIII (Invitrogen) before the mutant gene was ligated into the plasmid. Residue Val425 is at the end of subdomain I in the *Mtu*IPMS structure.

Plasmids containing the *Nme*IPMS, *Mtu*IPMS, and truncated α-IPMS genes were transformed into chemically competent *Escherichia coli* BL21(DE3)Star (*N. meningitidis* enzymes) or Rosetta 2 (*M. tuberculosis* enzymes) cell lines for expression.

Purification. Sterile LB was inoculated with 20 mL from an overnight culture and incubated at 37 °C until an OD_{600} of 0.4−0.8 was reached. The culture was then cooled to 20 °C for 30 min and induced with 0.5 mM isopropyl β-D-1-thiogalactopyranoside (IPTG). The culture was grown for 20 h at 20 °C. All proteins were expressed with N-terminal His tags.

Cells were harvested by centrifugation at 14000*g* for 30 min and resuspended in buffer A [50 mM potassium phosphate and 300 mM KCl (pH 8.0)] before being lysed by sonication. The soluble fraction was separated by centrifugation at 27000*g* for 30 min and passed through 5 mL Talon Superflow Metal Affinity resin (for *Nme*IPMS, *Nme*E365Term, and *Mtu*IPMS purifications and for *Mtu*LeuA425 used in WaterLOGSY and ITC) or a 5 mL HiTrap Ni affinity column (for *Mtu*LeuA425 used for crystallization). The resin was washed with buffer A, and protein eluted with buffer B [buffer A with 150 mM imidazole (pH 8.0)]. Protein-containing fractions were desalted, and dithiothreitol (DTT, 1 mM) and ethylenediaminetetraacetic acid (EDTA, 0.5 mM) were added.

The polyhistidine tag was removed by 4 °C overnight incubation with tobacco etch virus (TEV) protease, leaving the proteins with an N-terminal extension (GIDPFT for the *N. meningitidis* enzymes and GA in the *M. tuberculosis* enzymes). DTT and EDTA were removed from the solution on a desalting column. TEV protease and the cleaved His tag were then separated from the protein of interest using metal affinity chromatography as described above, and the desired fractions were pooled. Proteins were further purified by gel

dx.doi.org/10.1021/bi201717j | *Biochemistry* 2012, 51, 2289−2297

filtration chromatography on a Sephacryl 200 16/60 column (GE Healthcare) in buffer consisting of 50 mM bis-tris-propane (BTP, pH 7.0) for *Nme*IPMS and in buffer consisting of 25 mM Tris-HCl (pH 7.5), 125 mM NaCl, and 5 mM KCl for *Mtu*IPMS. Enzyme-containing fractions were identified by gel electrophoresis as a major band, which corresponded well with the calculated molecular weights, then pooled, and stored at −80 °C at 5−10 mg/mL.

Experiments with *E. coli* BW25113 ΔLeuA::kan Cells. *E. coli* BW25113 ΔLeuA::kan cells from the Keio collection[16] were obtained from W. Patrick at Massey University (Albany, New Zealand). These cells lack the *leuA* gene, which encodes α-IPMS, and are leucine auxotrophs. The *leuA* gene has been replaced with a gene conferring resistance to the antibiotic kanamycin. Plates of M9 minimal agar were spread with BW25113 ΔLeuA::kan cells that had been transformed with pFH01, pE365Term, pProExHTa-LeuA, or pProExHTa-LeuA425. After overnight incubation at 37 °C, cell growth was assessed to determine whether these plasmids could rescue α-IPMS expression. Positive and negative controls were performed by incubating BW25113 ΔLeuA::kan on M9 minimal agar in the presence and absence of 0.6 mg/mL leucine.

4,4′-Dithiodipyridine-Coupled Assays at 324 nm. Initial velocity data were obtained using 4,4′-dithiodipyridine (DTP) to detect the formation of CoASH product (ε = 1.98 × 10^4 L mol^{-1} cm^{-1}) at 324 nm and 25 °C. A typical reaction involved an assay solution containing 250 μM AcCoA, 250 μM α-KIV, 100 μM DTP, 20 mM KCl, and 20 mM $MgCl_2$ in 1 mL of 50 mM HEPES (pH 7.5) in a quartz cuvette, at the required temperature, and was initiated by addition of purified enzyme to a concentration of 10 nM. Assays investigating uncoupled hydrolysis used no α-KIV and an increased protein concentration of 3.3 μM. All kinetic measurements were performed in duplicate, and the typical error was less than 10%. Apparent K_M values were determined by varying one substrate while holding the other at a concentration of 250 μM and fitting rates to the Michaelis−Menten equation using Grafit.[17]

Crystallization. Fresh samples of the two truncated proteins were subjected to sitting drop vapor diffusion crystallization trials using a Cartesian HoneyBee robot.[18] A 100 nL volume of *Nme*E365Term protein [7.5 mg/mL in 50 mM BTP buffer (pH 7.0)] was mixed with 100 nL of each of 480 crystallization solutions from an in-house screen. Small crystals of *Nme*E365Term were observed under multiple conditions of the robotic screen. Large, well-diffracting crystals were produced in larger sitting drop experiments (1 + 1 μL drops) using a crystallization solution containing 0.2 M magnesium acetate and 18% mPEG 3350. Similarly, *Mtu*LeuA425 protein [3.5 mg/mL in buffer containing 25 mM Tris-HCl (pH 7.5), 125 mM NaCl, and 5 mM KCl] was crystallized under various screen conditions that were optimized in a final crystallization solution containing 24% PEG 3350 and 275 mM lithium nitrate using protein solution in 1 + 1 μL sitting drops. Crystals of a fully occupied α-KIV complex were obtained by soaking *Mtu*LeuA425 crystals in the crystallization solution supplemented with 5 mM $MnCl_2$ and 5 mM α-KIV. Cocrystallization methods were used for *Mtu*IPMS but yielded either poor diffraction quality crystals or no new information.

All crystals were flash-frozen in liquid nitrogen after a brief 10−20 s soak in crystallization solution supplemented with 15% glycerol, or for the α-KIV complex, with a solution supplemented with 15% glycerol, 5 mM $MnCl_2$, and 5 mM α-KIV. Diffraction data for *Nme*E365Term were collected at Australian Synchrotron beamline MX2 using the BlueIce software package.[19] Diffraction data for *Mtu*LeuA425 crystals were collected on a Rigaku MicroMax-007 HR rotating anode instrument equipped with a MarResearch Mar345dtb detector and Oxford Cryosystem Cobra cooling system. Data collection statistics are summarized in Table 2.

Structure Determination and Refinement. Diffraction data were processed using *XDS*[20] for *Nme*E365Term and *MOSFLM*[21] for *Mtu*LeuA425 and were scaled with *SCALA*.[22] Both structures were determined by molecular replacement, the *Nme*E365Term structure using BALBES[23] and the *Mtu*LeuA425 structure using PHASER,[24] with an appropriately truncated version of the *Mtu*IPMS structure [Protein Data Bank (PDB) entry 1SR9], minus all ligands, ions, and water molecules, taken as a search model. The models were completed with iterative cycles of manual building with *Coot*[25] and refinement with *REFMAC*.[26] The active site electron density was closely inspected, and appropriate metal atoms and ligands were included in the refinement. Finally, solvent molecules were added by automatic peak picking from $F_o - F_c$ electron density maps using *Coot*. Peaks above 3σ were selected, and water molecules were manually checked in *Coot*. Refinement statistics are listed in Table 2. Final coordinates for *Nme*E365Term and *Mtu*LeuA425 (with and without α-KIV) have been deposited in the Protein Data Bank as entries 3RMJ, 3U6W, and 3HPX, respectively.

WaterLOGSY NMR. Water ligand observed via gradient spectroscopy (WaterLOGSY) ^{1}H NMR spectra were recorded on a DRX 400 spectrometer (Bruker) operating at 400 MHz and 25 °C. For wild-type and truncated *Mtu*IPMS, samples consisted of 2 mM α-KIV, 3 mM $MgCl_2$, 3 mM KCl, 10% (v/v) D_2O, and 10 mM HEPES (pH 7.5). For wild-type and truncated *Nme*IPMS, samples consisted of 2 mM α-KIV, 3 mM $MgCl_2$, 10% (v/v) D_2O, and 10 mM HEPES (pH 7.5). A WaterLOGSY spectrum was first collected on each sample in the absence of enzyme. Enzyme was then added to a final concentration of ∼25 μM, and a second spectrum was recorded. The WaterLOGSY pulse program followed the published scheme[27] without a water flipback pulse. An initial water-selective 180° Gaussian pulse of 10 ms was used, and the NOE mixing time was 1 s. During the double spin−echo scheme used for water suppression, the water-selective 180° pulses were 2 ms. Spectra were collected with 400 scans. Chemical shifts are relative to external tetramethylsilane (TMS, 0 ppm).

Isothermal Titration Calorimetry. Isothermal titration calorimetry (ITC) was performed using a VP-ITC microcalorimeter (MicroCal). Protein samples were prepared by using ITC buffer [50 mM Tris (pH 7.5), 25 mM KCl, and 12 mM $MgCl_2$] in place of BTP buffer in the final gel filtration step of purification. Ligand solutions were prepared by dissolving α-KIV in a buffer identical to that of the protein (i.e., from the same batch). Protein and ligand solutions were degassed under vacuum for at least 5 min before being used. Protein (1.46 mL) was placed in the calorimeter sample cell, and the calorimeter syringe was filled with 250 μL of α-KIV. The protein concentration was 20 μM for *Mtu*IPMS experiments and 100 μM for *Mtu*LeuA425 experiments, with α-KIV concentrations of 350 and 150 μM for *Mtu*IPMS and *Mtu*LeuA425, respectively. A ligand solution (10 uL) was injected into the sample cell every 400 s at 20 °C. K_D values were found by fitting data to the One Set of Sites model in Origin 7.0.[28]

dx.doi.org/10.1021/bi201717j | *Biochemistry* 2012, 51, 2289−2297

Table 1. Kinetic Data for *Nme*IPMS, *Nme*E365Term, and *Mtu*IPMS[a]

	*Nme*IPMS[9]	*Nme*E365Term[9]	*Mtu*IPMS[29]	*Mtu*LeuA425
normal catalysis				
K_M^{app} (μM) for α-KIV	30 ± 2	–	12 ± 1	–
K_M^{app} (μM) for AcCoA	35 ± 3	–	136 ± 5	–
k_{cat} (s^{-1})	13 ± 0.3	–	3.5 ± 0.1	–
uncoupled AcCoA hydrolysis[b]				
K_M^{app} (μM) for AcCoA	250 ± 30	150 ± 20	160 ± 29	–
k_{cat} (s^{-1})	0.011 ± 0.001	0.010 ± 0.001	0.03 ± 0.002	–

[a]No activity was found for *Mtu*LeuA425 at concentrations up to 3 μM. [b]Hydrolysis of AcCoA in the absence of α-KIV.

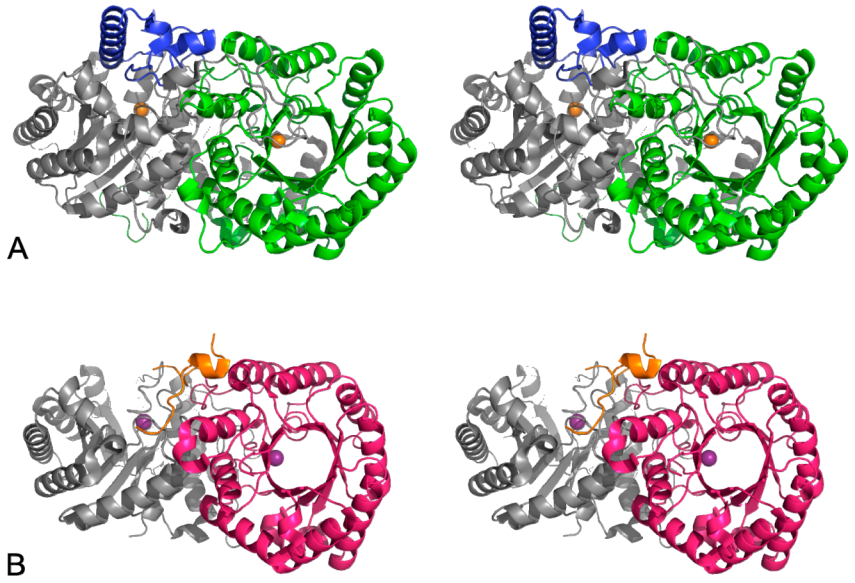

Figure 3. Stereo representations of crystal structures of truncated α-IPMS variants, one monomer of each colored gray and the other color-coded by domain. (A) *Mtu*LeuA425 at 2.03 Å: green for the catalytic domain, blue for subdomain I, and orange for Ni^{2+}. (B) *Nme*E365Term at 1.95 Å: pink for the catalytic domain, orange for subdomain I, and purple for Mn^{2+}. Much of subdomain I is undefined in *Nme*E265Term.

RESULTS

Cloning and Purification of α-IPMS Variants. A truncated variant of *Nme*IPMS was generated by introducing a stop codon, at Glu365, into the gene encoding the full-length protein. The expressed, truncated protein (*Nme*E365Term) lacks the C-terminal allosteric regulatory domain of the wild-type enzyme. The variant *Mtu*LeuA425, which similarly truncates *Mtu*IPMS, was generated by amplification of the gene corresponding to residues 1–425 from the plasmid bearing the full *Mtu*IPMS gene.[15] Constructs for the expression of both these truncated proteins were confirmed by sequencing of the expression plasmids and by the reduced size of the expressed proteins relative to their wild-type counterparts (Figure S1 and Table S1 of the Supporting Information).

Size exclusion chromatography indicated that both wild-type proteins and their shortened counterparts are homodimeric and that wild-type *Nme*IPMS remains homodimeric in the presence of the allosteric inhibitor leucine (Figure S2 and Table S2 of the Supporting Information). This is consistent with previous studies showing the *Mtu*IPMS is also a dimer in the presence or absence of leucine.[29] *Mtu*IPMS and *Nme*IPMS have 78% identical sequences.

Kinetic Characterization of the Catalytic Domains of *Nme*IPMS and *Mtu*IPMS. Neither of the truncated variants was able to catalyze the condensation of AcCoA and α-KIV, although *Nme*E365Term was shown to hydrolyze AcCoA in a manner that was independent of the presence of α-KIV (Table 1). As expected, the hydrolytic activity of this truncated variant was not affected by the presence of leucine.[9] No uncoupled hydrolysis of AcCoA was observed for *Mtu*LeuA425.

The α-IPMS reaction involves addition of the acetyl group to C2 of α-KIV, which is followed by hydrolysis of the AcCoA thioester.[29] This hydrolysis is part of the normal catalytic cycle, and it appears that the catalytic machinery responsible for this hydrolysis is able to function, at least partially, irrespective of the presence or absence of α-KIV.

Catalytic Activity of α-IPMS Variants in Vivo. *E. coli* BW25113 ΔLeuA::kan cells from the Keio collection[16] were used to probe the in vivo activity of the wild-type and truncated *N. meningitidis* and *M. tuberculosis* α-IPMS enzymes. These *E. coli* cells lack the *leuA* gene that encodes the native α-IPMS enzyme and are thus leucine auxotrophs. Growth of these cells is only supported by addition of leucine to the growth medium. BW25113 ΔLeuA::kan cells were transformed with pFH01, pE365Term, pProExHTa-LeuA, and pProExHTa-LeuA425 plasmids (encoding *Nme*IPMS, *Nme*E365Term, *Mtu*IPMS, and *Mtu*LeuA425, respectively) and grown on minimal medium. Cell lines that grew on this medium indicated that the relevant wild-type enzyme was able to perform adequately as an α-IPMS in place of the native *E. coli* enzyme. Both full-length *Nme*IPMS and *Mtu*IPMS supported growth of the *leuA* deficient cells on M9 minimal medium in the absence of added leucine, whereas the two truncated enzymes, *Nme*E365Term and *Mtu*LeuA425, did not support bacterial growth (Figure S3

dx.doi.org/10.1021/bi201717j | *Biochemistry* 2012, 51, 2289–2297

of the Supporting Information). These observations are consistent with the severe attenuation of α-IPMS activity of the truncated enzymes found in vitro.

Crystal Structures of *Nme*E365Term and *Mtu*LeuA425. Crystal structures (Figure 3) of the truncated variants *Nme*E365Term (at 1.95 Å resolution) and *Mtu*LeuA425 (at 2.03 Å resolution) were determined by molecular replacement using the *Mtu*IPMS structure (PDB entry 1SR9[8]), which is the full-length α-IPMS from *M. tuberculosis* bound to substrate α-KIV. Both crystal structures were found to contain a dimer in the asymmetric unit. Full details of data collection and refinement are provided in Table 2.

In *Nme*E365Term (PDB entry 3RMJ), each monomer comprised residues 1−364 of the full-length protein, with residues 4−296 and 311−324 being modeled for chain A and residues 4−297 and 311−324 for chain B; no interpretable electron density could be found for the remaining residues, which were presumed to be disordered. By analogy with the full-length *Mtu*IPMS structure, the majority of the missing residues from *Nme*E365Term are from subdomain I, which crosses over in the dimer and sits over the active site of the other monomer. A Mn^{2+} ion is present in each of the two active sites. In the *Mtu*LeuA425 structure (PDB entry 3HPX), which comprises residues 1−425 of the full-length protein, all residues could be modeled apart from residues 1−18 of chain A and residues 1−17 of chain B. A Ni^{2+} ion is present in each of the *Mtu*LeuA425 monomers, presumably acquired from the Ni affinity chromatography purification step.

The two truncated structures, *Nme*E365Term and *Mtu*LeuA425, can be superimposed with a root-mean-square difference (rmsd) in Cα position of 1.73 Å for 490 common residues of the dimer. As may be expected, the *Mtu*LeuA425 structure aligns closely with the corresponding portion of full-length *Mtu*IPMS (rmsd of 0.26 Å for 698 residues of the dimer), whereas *Nme*E365Term is less well aligned with full-length *Mtu*IPMS (rmsd of 1.78 Å for 447 residues). In *Nme*E365Term, much of subdomain I is undefined: residues 297−310, 325, and 326 in chain A and residues 298−310, 325, and 326 in chain B. Residues 311−324 in each monomer are significantly displaced; the Cα of conserved residue Tyr313, present in the active site of the *M. tuberculosis* enzymes, is 14.1 Å (chain A) and 14.3 Å (chain B) from the equivalent Tyr410 in *Mtu*IPMS. In *Mtu*LeuA425, the corresponding residues (408−421) are located in the same position as in *Mtu*IPMS, but in *Nme*E365Term, they are arranged along the interface of the $(\beta/\alpha)_8$ barrel monomers.

The active sites of *Nme*E365Term and *Mtu*LeuA425 correspond very closely to that of α-KIV-bound, wild-type *Mtu*IPMS, with one clear difference. In the wild-type enzyme, a Zn^{2+} ion is coordinated to two oxygens in α-KIV, a water molecule, and the side chains of three residues: Asp81, His285, and His287. The coordinated amino acid side chains are themselves stabilized by hydrogen bonds to Asn321, Glu309, and Gly320, respectively (Figure 4A). The divalent metal ion in the variants (Ni^{2+} in *Mtu*LeuA425 and Mn^{2+} in *Nme*E365Term) is farther from the α-KIV binding site of the wild type and coordinates with two water molecules and four amino acid side chains in each protein: Asp16, His204, His206, and Asn240 in *Nme*E365Term and Asp81, His285, His287, and Asn321 in *Mtu*LeuA425 (Figure 4B,C). These changes accompany a significant displacement of the metal ion: in *Nme*E365Term, the Mn^{2+} ion is 2.2 Å from the equivalent position of the Zn^{2+} ion of *Mtu*IPMS, and the Ni^{2+} ion in

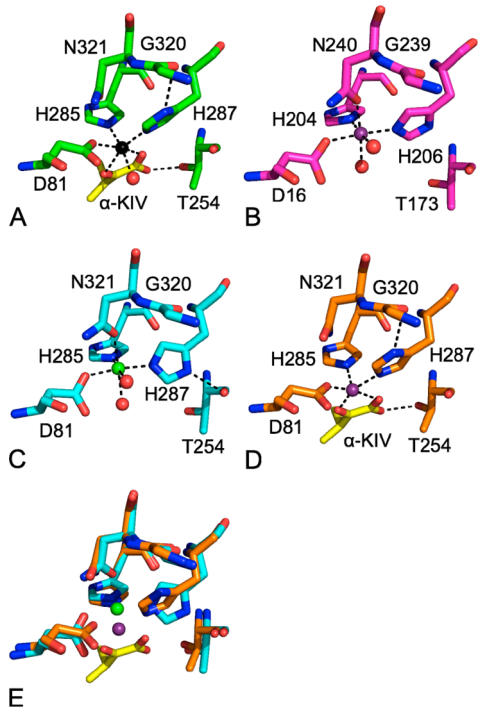

Figure 4. α-KIV binding sites in *Mtu*IPMS (A, PDB entry 1SR9,[8] green), *Nme*E365Term (B, PDB entry 3RMJ, magenta), and *Mtu*LeuA425 (C, PDB entry 3HPX, cyan; D, PDB entry 3U6W, orange). The metal ion (Zn^{2+}, black; Ni^{2+}, green; Mn^{2+}, purple) coordinates with four residues in unliganded enzymes, but with only three in the presence of α-KIV. (E) Overlay of panels C and D (waters excluded for the sake of clarity).

*Mtu*LeuA425 is 1.9 Å distant. This change in the position of the metal ion appears to be associated with the conformational change of an active site histidine residue. In *Mtu*LeuA425, His287 is rotated so that it forms a hydrogen bond with the main chain carbonyl oxygen of Thr254 rather than that of Gly320. His206 in *Nme*E365Term is also rotated, but not quite far enough to form similar hydrogen bonding.

To assess the effect of substrate binding on metal position, *Mtu*LeuA425 crystals were soaked with α-KIV and Mn^{2+} to give a crystal structure for the *Mtu*LeuA425−α-KIV complex (Table 2). This structure comprises the same residues as for the nonliganded structure, but with residues 392−398 from chain A and 396−398 from chain B missing and presumed disordered. It has one Mn^{2+} ion and one α-KIV molecule in each active site. This α-KIV complex structure has an rmsd in Cα positions of 0.21 Å for 756 residues when compared with the nonliganded *Mtu*LeuA425 and an rmsd of 0.24 Å for 668 residues when compared with *Mtu*IPMS. The active site residues in α-KIV-bound *Mtu*LeuA425 shift to allow the metal ion to bind in the same position as seen in the substrate-bound, wild-type enzyme (Figure 4D). We conclude that the altered metal position observed in the unliganded structures is due to the lack of α-KIV, rather than the lack of the regulatory domain.

Removal of the regulatory domain also appears to increase the flexibility of subdomain I of α-IPMS, comprising residues 369−424 in *M. tuberculosis* and residues 292−326 in *N. meningitidis*. This is particularly evident in residues 391−400 of *M. tuberculosis* α-IPMS, which are part of a pair of helices near the AcCoA binding site and have different degrees of flexibility in each monomer of the asymmetric protein dimer. Average *B* factors in *Mtu*IPMS for this region are 1.8 and 1.6 times greater

dx.doi.org/10.1021/bi201717j | *Biochemistry* 2012, 51, 2289−2297

Table 2. Crystallographic Data for *Nme*E365Term and *Mtu*LeuA425

	*Nme*E365Term	*Mtu*LeuA425	α-KIV-bound *Mtu*LeuA425
	λ = 0.9546 Å	λ = 1.5418 Å	λ = 1.5418 Å
		Data Collection	
space group	$P2_12_12_1$	$P1$	$P1$
unit cell parameters			
a, *b*, *c* (Å)	46.3, 103.6, 129.9	48.0, 70.9, 70.0	47.7, 70.6, 69.9
α, β, γ (deg)	90, 90, 90	62.5, 81.4, 70.3	62.29, 81.26, 70.16
resolution[a] (Å)	21.8−1.95 (2.06−1.95)	30−2.0 (2.1−2.0)	30−2.2 (2.3−2.2)
total no. of reflections	300624	357799	110119
no. of unique reflections	46485	47066	35261
completeness[a] (%)	99.9 (100.0)	94.5 (84.7)	93.2 (72.6)
I/σ[a]	12.3 (3.0)	17.8 (3.8)	12.1 (3.7)
multiplicity[a]	6.5	7.6	3.1
R_{merge}[a] (%)	11.9 (61.2)	12.6 (48.9)	11.6 (27.8)
		Refinement	
R (%)	15.8	17.4	22.5
R_{free} (%)	19.1	23.8	29.8
no. of amino acids	307 + 308 residues, 4731 atoms	407 + 408 residues, 6285 atoms	406 + 407 residues, 6346 atoms
no. of water molecules	332	633	160
other	2 Mn^{2+}, 2 Mg^{2+}, 5 glycerol	2 Ni^{2+}, 2 glycerol	2 Mn^{2+}, 2 α-KIV, 2 glycerol
average *B* factor (Å^2)			
protein	21.5	17.6	11.9
water	28.6	24.8	8.9
other	39.3	19.6	17.3
rmsd from target values			
bond lengths (Å)	0.017	0.019	0.018
bond angles (deg)	1.45	1.66	1.66
dihedral angles (deg)	6.21	6.66	7.16
Ramachandran plot (%)			
most favored	97.7	97.2	96.8
allowed	2.1	2.8	3.2
disallowed	0.2	0.0	0.0
PDB entry	3RMJ	3HPX	3U6W

[a]Figures in parentheses are for the outermost shell.

than the average values for β-barrel residues in the structure in chains A and B, respectively. Average *B* factors for this region in unliganded *Mtu*LeuA425 are 2.9 and 2.7 times greater than the average values for the β-barrel residues in chains A and B, respectively. In the full-length structure, there is significant asymmetry between the two monomers with respect to this region. Thus, the regulatory domain may act to maintain the inequality in flexibility between the two monomers. These same residues (391−400) are partially disordered in α-KIV-bound *Mtu*LeuA425 and fall within the large undefined regions of *Nme*E365Term.

WaterLOGSY NMR Spectroscopy. The NMR technique WaterLOGSY was used as a rapid screening method to examine whether α-KIV binds to the truncated variants. WaterLOGSY experiments allow the detection of binding of small molecules to protein targets with dissociation constants in the low micromolar to millimolar range.[27,30] The WaterLOGSY signal is produced by the selective transfer of bulk water magnetization to ligand in solution via the protein−ligand complex. In the resulting spectra, compounds that bind generally have signals with opposite sign relative to those of compounds that do not bind.

WaterLOGSY ^{1}H NMR spectra were recorded for α-KIV in the absence and presence of the wild-type and truncated variants of *Nme*IPMS and *Mtu*IPMS (Figure 5). Addition of both wild-type and truncated forms of the two enzymes produced a change in sign of the α-KIV WaterLOGSY ^{1}H NMR signals. This indicates that the truncated variants retain the ability to bind α-KIV in solution. In the presence of both *Nme*IPMS enzymes, the enhancement of the α-KIV signals is significantly greater than that seen for the *Mtu*IPMS variants. This could result from the tighter binding of α-KIV to *Mtu*IPMS, consistent with the lower K_M of this enzyme, as slow dissociation rates of the protein−ligand complex may limit the transfer of magnetization to the bulk ligand during the WaterLOGSY experiment.[31]

Isothermal Titration Calorimetry. ITC experiments were used to quantitatively analyze α-KIV binding in *Mtu*IPMS and *Mtu*LeuA425. The *M. tuberculosis* enzymes were chosen for these experiments as they were determined to be stable under ITC conditions. These experiments (Figure 6) show that α-KIV binding takes place for both wild-type and truncated proteins, with K_D values of 15 ± 3 μM for *Mtu*IPMS and 120 ± 15 nM for *Mtu*LeuA425. The lower K_D for the truncated variant indicates that α-KIV binds significantly more tightly to the noncatalytically active truncated enzyme than to the wild-type *Mtu*IPMS, in line with the trends seen in the WaterLOGSY experiments.

DISCUSSION

Whereas in some enzymes it is possible to create a feedback-independent enzyme by removal of a structurally distinct

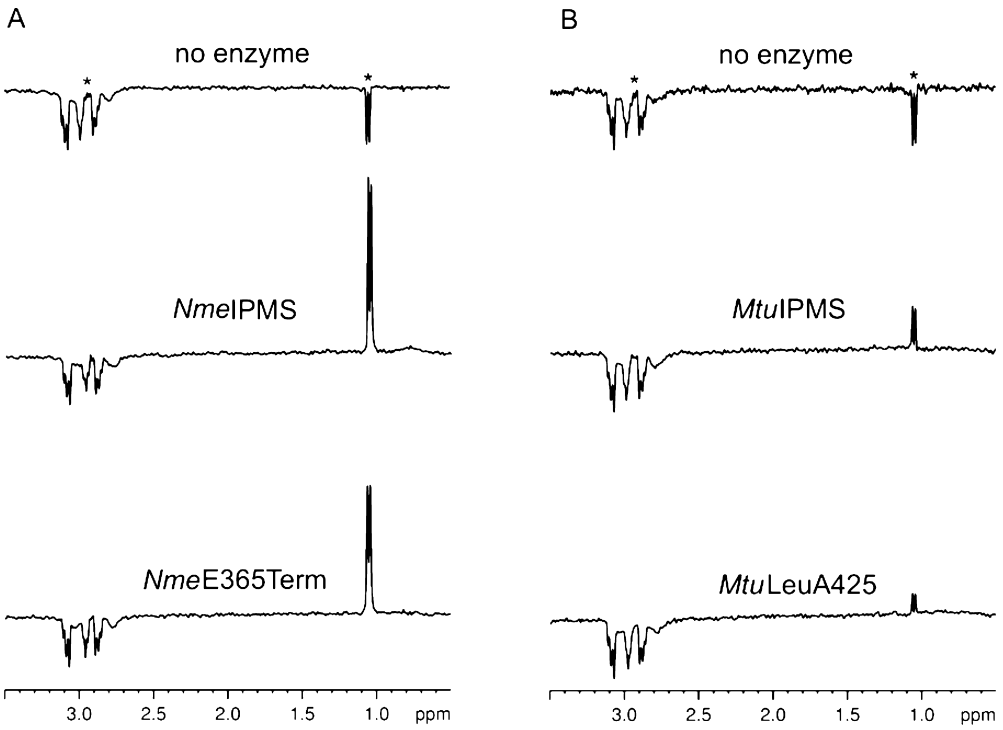

Figure 5. WaterLOGSY ^{1}H NMR experiments showing that the truncated variants of (A) *Nme*IPMS and (B) *Mtu*IPMS are able to bind α-KIV. Spectra of 2 mM α-KIV were recorded in the absence of enzyme (top), in the presence of 25 μM *Nme*IPMS or *Mtu*IPMS (middle), or in the presence of 25 μM truncated variant *Nme*E365Term or *Mtu*LeuA425 (bottom). The ^{1}H NMR peaks of α-KIV are at 1.05 and 2.94 ppm for the methyl and methine protons, respectively, as indicated by asterisks on the top spectra. Remaining peaks at 3.2−2.7 ppm are due to HEPES buffer.

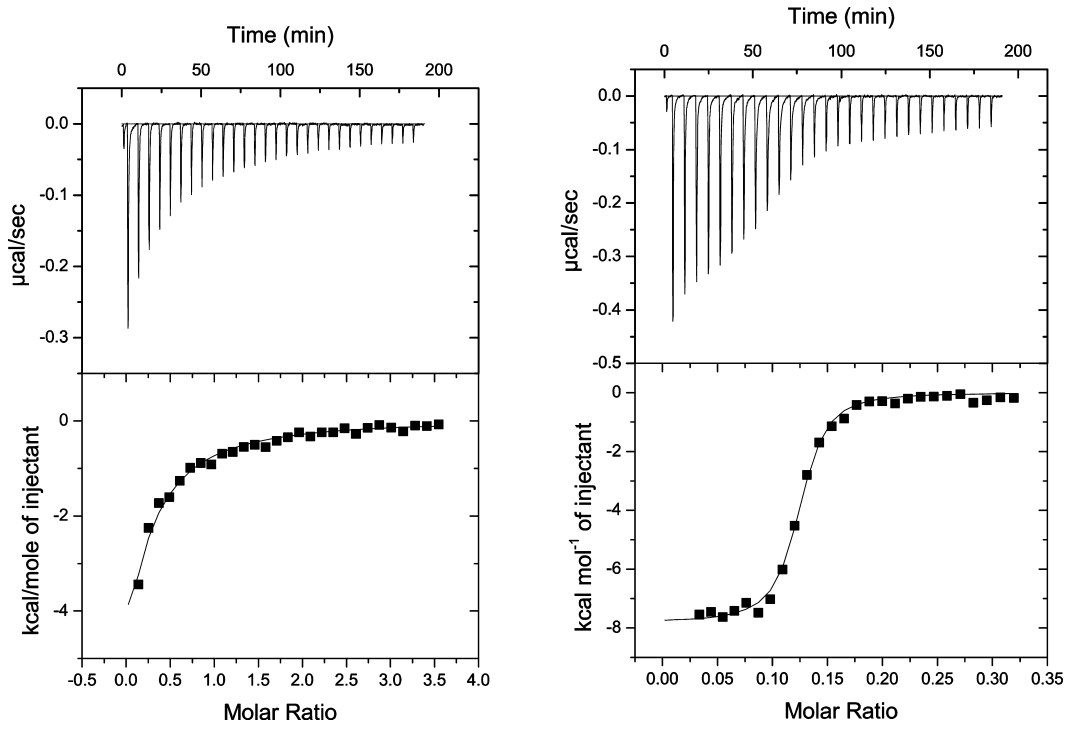

Figure 6. ITC data for 350 μM α-KIV titrated into 20 μM *Mtu*IPMS (left) and 150 μM α-KIV into 100 μM *Mtu*LeuA425 (right). Both data sets are fitted to the One Set of Sites model using Origin 7.

regulatory domain, for α-IPMS from *N. meningitidis* and *M. tuberculosis* such removal abolishes catalytic activity. In the absence of the regulatory domain, these enzymes are unable to catalyze the condensation of α-KIV and AcCoA to form α-IPM. Crystal structures of the truncated enzymes from *M. tuberculosis* and *N. meningitidis* show little overall difference from the wild-type enzyme, and the principal components of the active sites are intact. The small differences that can be inferred from the crystal structures provide some insight into the changes undergone by the active site upon α-KIV binding and suggest

dx.doi.org/10.1021/bi201717j | *Biochemistry* 2012, 51, 2289−2297

that dynamic fluctuations are critical for competent catalysis in α-IPMS.

In both *Nme*E365Term and *Mtu*LeuA425 (without α-KIV bound), the divalent metal ion in the active site has moved significantly compared to its position in wild-type, α-KIV-bound *Mtu*IPMS. This essential metal ion coordinates with the carbonyl groups of α-KIV and is proposed to activate the substrate for nucleophilic attack by the acetyl group of AcCoA.[29] A structure of α-KIV-bound *Mtu*LeuA425 shows the metal shifted back to its position in the wild-type structure, suggesting that this metal ion changes its position and coordination upon substrate binding.

The second key area of change between the wild-type and truncated structures is in subdomain I. This subdomain sits over the putative AcCoA binding site and could be key for positioning this substrate properly for catalysis. Analysis of the temperature factors from the crystal structures shows that there is some increase in the relative flexibility of subdomain I in the truncated *Mtu*LeuA425 compared to full-length *Mtu*IPMS. This region is undefined or, in the case of residues 311−324, displaced from its likely wild-type position near the active site in *Nme*E365Term. It appears that the regulatory domain acts to anchor the structure of this region in *Nme*IPMS. Subdomain I is one of the areas identified as having increased exposure to solvent in the *Mtu*IPMS variant Y410F.[14] This variant appears to be constitutively inhibited and has only 10% of the catalytic activity of the wild-type enzyme. Subdomain I of the leucine-bound *Mtu*IPMS also appears to exhibit increased flexibility when compared with the unbound structure,[8] although hydrogen−deuterium exchange shows no change in exposure to solvent for this region upon leucine binding.[14] It appears that minor changes in dynamic fluctuation in subdomain I can attenuate catalysis and could represent the in vivo signal transmission mechanism for feedback inhibition. The lack of catalytic activity of the truncated variants may also be associated with changes in the flexibility of this region of the protein. Given the likelihood that subdomain I provides some key hydrogen bonds to AcCoA, it is possible that the altered flexibility of this region of the protein may significantly disrupt the correct binding of AcCoA. Even so, the observation that *Nme*E365Term does catalyze the α-KIV-uncoupled hydrolysis demonstrates that this protein can bind and hydrolyze the thioester, in the absence of coupling to α-KIV.

In summary, these studies show two key insights into α-IPMS catalysis: (1) that a divalent metal ion may bind in one of two positions within the active site depending on the presence of substrate and (2) that the regulatory domain in α-IPMS is necessary for the catalytically competent dynamic fluctuations of subdomain I and the active site. The presence and structure of the subdomains and regulatory domain are critical for active site function in ways not apparent from crystal structures.

■ ASSOCIATED CONTENT

Supporting Information

Mass spectroscopy, sodium dodecyl sulfate−polyacrylamide gel electrophoresis, and analytical size exclusion chromatography data for wild-type and truncated α-IPMS enzymes and the growth of *E. coli* BW25113 ΔLeuA::kan cell lines. This material is available free of charge via the Internet at http://pubs.acs.org.

■ AUTHOR INFORMATION

Corresponding Author

*E.J.P.: Department of Chemistry, University of Canterbury, Private Bag 4800, Christchurch, New Zealand; telephone, (+64) 3 364 5682; fax, (+64) 3 364 2110; e-mail, emily.parker@canterbury.ac.nz. C.J.S.: School of Biological Sciences, University of Auckland, P.O. Box 92019, Auckland, New Zealand; telephone, (+64) 9 373 7599; e-mail, c.squire@auckland.ac.nz.

Funding

This research was supported by the Health Research Council of New Zealand and by funding from the Maurice Wilkins Centre for Molecular Biodiscovery.

Notes

The authors declare no competing financial interest.

■ ACKNOWLEDGMENTS

X-ray data collection for *Nme*E365Term was undertaken on beamline MX2 at the Australian Synchrotron (Victoria, Australia). We are grateful to Wayne Patrick for providing the *E. coli* BW25113 ΔLeuA::kan cells from the Keio collection.

■ ABBREVIATIONS

α-IPMS, α-isopropylmalate synthase; α-KIV, α-ketoisovalerate; AcCoA, acetyl-coenzyme A; α-IPM, (*S*)-α-isopropylmalate; *Mtu*IPMS, *M. tuberculosis* α-IPMS; *Nme*IPMS, *N. meningitidis* α-IPMS; *Nme*E365Term, truncated *N. meningitidis* α-IPMS; *Mtu*LeuA425, truncated *M. tuberculosis* α-IPMS; IPTG, isopropyl β-D-1-thiogalactopyranoside; DTT, dithiothreitol; EDTA, ethylenediaminetetraacetic acid; TEV protease, tobacco etch virus protease; BTP, bis-tris-propane; DTP, 4,4′-dithiodipyridine; HEPES, 4-(2-hydroxyethyl)-1-piperazineethanesulfonic acid; WaterLOGSY, water ligand observed via gradient spectroscopy; NOE, nuclear Overhauser effect; TMS, tetramethylsilane; ITC, isothermal titration calorimetry; rmsd, root-mean-square difference.

■ REFERENCES

(1) Mattevi, A., Bolognesi, M., and Valentini, G. (1996) The allosteric regulation of pyruvate kinase. *FEBS Lett. 389*, 15−19.

(2) Cho, Y., Sharma, V., and Sacchettini, J. C. (2003) Crystal structure of ATP phosphoribosyltransferase from *Mycobacterium tuberculosis*. *J. Biol. Chem. 278*, 8333−8339.

(3) Cross, P. J., Dobson, R. C., Patchett, M. L., and Parker, E. J. (2011) Tyrosine latching of a regulatory gate affords allosteric control of aromatic amino acid biosynthesis. *J. Biol. Chem. 286*, 10216−10224.

(4) de Kraker, J. W., and Gershenzon, J. (2011) From amino acid to glucosinolate biosynthesis: Protein sequence changes in the evolution of methylthioalkylmalate synthase in *Arabidopsis*. *Plant Cell 23*, 38−53.

(5) Leary, T. R., and Kohlhaw, G. B. (1972) α-Isopropylmalate synthase from *Salmonella typhimurium*. Analysis of the quaternary structure and its relation to function. *J. Biol. Chem. 247*, 1089−1095.

(6) de Carvalho, L. P., Argyrou, A., and Blanchard, J. S. (2005) Slow-onset feedback inhibition: Inhibition of *Mycobacterium tuberculosis* α-isopropylmalate synthase by L-leucine. *J. Am. Chem. Soc. 127*, 10004−10005.

(7) Pátek, M., Krumbach, K., Eggeling, L., and Sahm, H. (1994) Leucine synthesis in *Corynebacterium glutamicum*: Enzyme activities, structure of leuA, and effect of leuA inactivation on lysine synthesis. *Appl. Environ. Microbiol. 60*, 133−140.

(8) Koon, N., Squire, C. J., and Baker, E. N. (2004) Crystal structure of LeuA from *Mycobacterium tuberculosis*, a key enzyme in leucine biosynthesis. *Proc. Natl. Acad. Sci. U.S.A. 101*, 8295−8300.

(9) Huisman, F. H., Hunter, M. F., Devenish, S. R., Gerrard, J. A., and Parker, E. J. (2010) The C-terminal regulatory domain is required for catalysis by *Neisseria meningitidis* α-isopropylmalate synthase. *Biochem. Biophys. Res. Commun. 393*, 168−173.
(10) Kohlhaw, G. B., Leary, T. R., and Umbarger, H. E. (1969) α-Isopropylmalate synthase from *Salmonella typhimurium*. Purification and properties. *J. Biol. Chem. 244*, 2218−2225.
(11) de Carvalho, L. P., and Blanchard, J. S. (2006) Kinetic analysis of the effects of monovalent cations and divalent metals on the activity of *Mycobacterium tuberculosis* α-isopropylmalate synthase. *Arch. Biochem. Biophys. 451*, 141−148.
(12) de Carvalho, L. P., Frantom, P., Argyrou, A., and Blanchard, J. (2009) Kinetic evidence for inter-domain communication in the allosteric regulation of α-isopropylmalate synthase from *Mycobacterium tuberculosis*. *Biochemistry 48*, 1996−2004.
(13) Cavalieri, D., Casalone, E., Bendoni, B., Fia, G., Polsinelli, M., and Barberio, C. (1999) Trifluoroleucine resistance and regulation of α-isopropyl malate synthase in *Saccharomyces cerevisiae*. *Mol. Gen. Genet. 261*, 152−160.
(14) Frantom, P. A., Zhang, H. M., Emmett, M. R., Marshall, A. G., and Blanchard, J. S. (2009) Mapping of the allosteric network in the regulation of α-isopropylmalate synthase from *Mycobacterium tuberculosis* by the feedback inhibitor L-leucine: Solution-phase H/D exchange monitored by FT-ICR mass spectrometry. *Biochemistry 48*, 7457−7464.
(15) Koon, N., Squire, C. J., and Baker, E. N. (2004) Crystallization and preliminary X-ray analysis of α-isopropylmalate synthase from *Mycobacterium tuberculosis*. *Acta Crystallogr. D60*, 1167−1169.
(16) Baba, T., Ara, T., Hasegawa, M., Takai, Y., Okumura, Y., Baba, M., Datsenko, K. A., Tomita, M., Wanner, B. L., and Mori, H. (2006) Construction of *Escherichia coli* K-12 in-frame, single-gene knockout mutants: The Keio collection. *Mol. Syst. Biol.,* 2.
(17) Leatherbarrow, R. J. (2007) *Grafit*, version 6, Erithacus Software Ltd., Horly, U.K.
(18) Moreland, N., Ashton, R., Baker, H. M., Ivanovic, I., Patterson, S., Arcus, V. L., Baker, E. N., and Lott, J. S. (2005) A flexible and economical medium-throughput strategy for protein production and crystallization. *Acta Crystallogr. D61*, 1378−1385.
(19) McPhillips, T. M., McPhillips, S. E., Chiu, H. J., Cohen, A. E., Deacon, A. M., Ellis, P. J., Garman, E., Gonzalez, A., Sauter, N. K., Phizackerley, R. P., Soltis, S. M., and Kuhn, P. (2002) Blu-Ice and the Distributed Control System: Software for data acquisition and instrument control at macromolecular crystallography beamlines. *J. Synchrotron Radiat. 9*, 401−406.
(20) Kabsch, W. (2010) *XDS*. *Acta Crystallogr. D66*, 125−132.
(21) Leslie, A. G. (2006) The integration of macromolecular diffraction data. *Acta Crystallogr. D62*, 48−57.
(22) Evans, P. (2006) Scaling and assessment of data quality. *Acta Crystallogr. D62*, 72−82.
(23) Long, F., Vagin, A. A., Young, P., and Murshudov, G. N. (2008) BALBES: A molecular-replacement pipeline. *Acta Crystallogr. D64*, 125−132.
(24) McCoy, A. J., Grosse-Kunstleve, R. W., Adams, P. D., Winn, M. D., Storoni, L. C., and Read, R. J. (2007) Phaser crystallographic software. *J. Appl. Crystallogr. 40*, 658−674.
(25) Emsley, P., Lohkamp, B., Scott, W. G., and Cowtan, K. (2010) Features and development of Coot. *Acta Crystallogr. D66*, 486−501.
(26) Murshudov, G. N., Skubak, P., Lebedev, A. A., Pannu, N. S., Steiner, R. A., Nicholls, R. A., Winn, M. D., Long, F., and Vagin, A. A. (2011) REFMAC5 for the refinement of macromolecular crystal structures. *Acta Crystallogr. D67*, 355−367.
(27) Dalvit, C., Fogliatto, G., Stewart, A., Veronesi, M., and Stockman, B. (2001) WaterLOGSY as a method for primary NMR screening: Practical aspects and range of applicability. *J. Biomol. NMR 21*, 349−359.
(28) *Origin 7*, OriginLab, Northhampton, MA, 2002.
(29) de Carvalho, L. P., and Blanchard, J. S. (2006) Kinetic and chemical mechanism of α-isopropylmalate synthase from *Mycobacterium tuberculosis*. *Biochemistry 45*, 8988−8999.
(30) Dalvit, C., Pevarello, P., Tatò, M., Veronesi, M., Vulpetti, A., and Sundstrom, M. (2000) Identification of compounds with binding affinity to proteins via magnetization transfer from bulk water. *J. Biomol. NMR 18*, 65−68.
(31) Dalvit, C., Fasolini, M., Flocco, M., Knapp, S., Pevarello, P., and Veronesi, M. (2002) NMR-based screening with competition water-ligand observed via gradient spectroscopy experiments: Detection of high-affinity ligands. *J. Med. Chem. 45*, 2610−2614.